Applied Surface Science 746 (2026) 167650

Contents lists available at ScienceDirect

Applied Surface Science

journal homepage: www.elsevier.com/locate/apsusc

Full Length Article

In-operando photoemission spectroscopy reveals gate-modulated amplification of ammonia sensitivity in flexible carbon nanotube based thin-film transistor

Christos Gatsios [a], Antonello Mascia [b], Anna Goncharenko [c], Cristian Tomasi Cebotari [a,d], Sahira Vasquez [c], Niko Münzenrieder [c], Giulia Elli [c], Zygmunt Milosz [e], Matteo Amati [e], Luca Gregoratti [e], Luca Pasquali [f,g,h], Piero Cosseddu [b], Luisa Petti [c], Marco V. Nardi [a,*], Melanie Timpel [a,*]

[a] *IMEM-CNR, Institute of Materials for Electronics and Magnetism, Trento unit c/o Fondazione Bruno Kessler, Via alla Cascata 56/C, 38123 Trento, Italy*
[b] *Department of Electrical and Electronics Engineering, University of Cagliari, Piazza D'Armi, 09123 Cagliari, Italy*
[c] *Faculty of Engineering, Free University of Bozen-Bolzano, Via Bruno Buozzi 1, 39100 Bolzano, Italy*
[d] *Department of Chemistry, Life Science and Environmental Sustainability, University of Parma, Parco Area delle Scienze 17/A, 43124 Parma, Italy*
[e] *Elettra Sincrotrone Trieste S.C.p.A., s.s. 14 km 163.5 in AREA Science Park, 34149 Trieste, Italy*
[f] *Department of Engineering "Enzo Ferrari", University of Modena and Reggio Emilia, Via Vivarelli 10, 41125 Modena, Italy*
[g] *CNR-Istituto Officina dei Materiali (IOM), Strada Statale 14, Km. 163.5 in AREA Science Park, Basovizza, 34149 Trieste, Italy*
[h] *Department of Physics, University of Johannesburg, P.O. Box 524, Auckland Park 2006, Johannesburg, South Africa*

ARTICLE INFO

Keywords:
Semiconducting single-walled carbon nanotubes
Gas–solid interfaces
In-operando surface spectroscopies
Flexible thin-film transistor
Electrochemical sensors

ABSTRACT

We report an *in-operando* X-ray photoelectron spectroscopy (XPS) study revealing gate-induced amplification of ammonia sensitivity in flexible carbon nanotube (CNT) thin-film transistors (TFTs). Using scanning photoemission microscopy (SPEM) under operating conditions, we directly probe surface charge-transfer processes at the CNT surface during NH_3 exposure while electrostatically modulating the carrier density in the transistor channel. Flexible CNT-TFTs fabricated on polyimide substrates operate at low voltages (± 5 V) and exhibit typical p-type behavior. Upon exposure to NH_3 at a nominal concentration of ~8 ppm, the C 1s core level shifts by ~0.5 eV toward higher binding energy in the unbiased state, consistent with electron donation from NH_3 to the CNT network. Strikingly, applying a −5 V gate bias approximately doubles the magnitude of this shift to ~1.0 eV, providing direct spectroscopic evidence that electrostatic gating enhances gas-induced charge transfer at the CNT surface. These findings reveal how transistor gating can modulate gas–surface interactions at the electronic level and demonstrate the capability of *in-operando* photoemission spectroscopy to uncover sensing mechanisms beyond conventional electrical measurements. The approach provides a pathway toward the rational design of flexible, low-power chemical sensors with tunable sensitivity.

1. Introduction

The development of flexible gas sensors is increasingly driven by applications in environmental monitoring, wearable and portable detection systems, and biomedical diagnostics [1]. Carbon nanotubes (CNTs) offer distinctive advantages over conventional metal-oxide sensors, mainly owing to their high mechanical flexibility and exceptionally high surface-to-volume ratio. The latter one maximizes the density of active sites and enables faster adsorption–desorption kinetics,[2–4] while also eliminating the need for elevated operating temperatures (300–450 °C) typically required for sensor recovery [5,6].

An important application of CNT-based sensors is the detection of ammonia (NH_3), both a significant health hazard and an environmental pollutant. According to occupational exposure limits, concentrations above 20 ppm are considered harmful [7]. Moreover, elevated NH_3 levels in the body are associated with various diseases, making early detection essential for preventing health complications [8–11]. Semiconducting single-walled CNTs, even without functionalization, are

* Corresponding authors.
E-mail addresses: marcovittorio.nardi@cnr.it (M.V. Nardi), melaniekristina.timpel@cnr.it (M. Timpel).

https://doi.org/10.1016/j.apsusc.2026.167650
Received 27 April 2026; Received in revised form 17 June 2026; Accepted 22 June 2026
Available online 23 June 2026

ideal active materials for NH_3 detection in such application scenarios, as they have demonstrated detection limits down to 2 ppm [3,4].

As diagnostic, environmental, and food-safety monitoring tools, NH_3 sensors must combine high sensitivity with portability and low production cost to enable widespread use [12–16]. Although CNT-based sensors have demonstrated excellent performance, their sensing behavior, particularly under operating conditions and within device-relevant architectures, remains insufficiently understood [16,17]. In most studies, sensing is assessed primarily through electrical measurements, from which the underlying gas–surface interactions are inferred indirectly, often without isolating the contributions of surface chemistry, device fabrication, and operating environment [4,15,16,18]. As a result, direct experimental insight into surface chemical phenomena such as gas adsorption, desorption, and charge-transfer during operation is often overlooked. This is largely because such investigations require advanced *in-situ* and *in-operando* surface-sensitive characterization techniques that are not commonly employed. However these methods can be essential for identifying fundamental performance limitations and guiding the rational improvement of device architectures [19–21].

To directly probe this process, our previous work employed *in-situ* X-ray photoelectron spectroscopy (XPS) during dynamic high pressure (DHP) dosing of NH_3, complemented by electrical measurements in dry air and under DHP dosing in ultra-high vacuum (UHV) conditions, correlating core-level shifts with the resistive response of spray-coated CNT thin films integrated in flexible chemoresistive devices.[22] Using this approach, hole depletion at the CNT surface was directly observed through shifts of the C 1s core levels towards higher binding energy (BE), resulting from charge transfer from electron-donating NH_3 to the p-type CNT network. This direct spectroscopic evidence explained the observed increase in device resistance upon exposure and is consistent with previous studies [2,4,23,24].

In the present study, we extend this approach by employing *in-operando* SPEM during NH_3 exposure in CNT-based thin-film transistors (CNT-TFTs). The key advancement over our previous two-terminal chemoresistive study [22] lies in the gate electrode, which provides independent electrostatic control over the charge carrier concentration and thus the Fermi level of the semiconducting CNT channel. By electrostatic gating, we can directly observe how the Fermi level position governs the efficiency of surface charge-transfer from adsorbed NH_3 molecules, a question inaccessible to purely electrical measurements. To the best of our knowledge, this is the first direct, surface-sensitive spectroscopic observation of gate-modulated gas–surface charge transfer in CNT-TFTs. While previous electrical studies have reported gate-induced amplification of gas sensitivity in transistor-type architectures, [25–27] these investigations have been largely restricted to electrical characterization, without direct, surface-sensitive chemical insight into the underlying gas–surface interactions.

Our *in-operando* approach combines the surface sensitivity of XPS with the electrostatic control provided by the TFTs configuration, allowing direct observation of gas-surface interactions under operating conditions. Our findings corroborate and extend recent electrical studies focused on gate-modulated sensitivity in similar devices, [26,27] providing direct spectroscopic evidence of the underlying charge transfer interactions, with the C 1s core-level shift increasing twofold upon ammonia exposure compared to the unbiased state. This method supports the investigation of gate-modulated charge-transfer interactions at gas–solid interfaces and can be generalized to various analyte gases and sensing materials, offering valuable insight into the origins and limitations of gas sensing in low-dimensional material systems.

2. Experimental

2.1. Device fabrication

The fabrication of the flexible CNT-TFT was performed on a 125-μm thick polyimide (PI) substrate, onto which a 50-nm thick aluminum layer was thermally evaporated through a shadow mask to form the gate electrode in a bottom-gate, bottom-contact device configuration, as shown in Fig. 1**a and 1b**. A 180-nm thick Parylene-C film was then deposited by chemical vapor deposition (CVD) to serve as the gate insulator, providing a uniform, pinhole-free layer. Next, source and drain electrodes were created by thermally evaporating a 50-nm thick gold film, followed by patterning using standard photolithography processes. The device channel length was about 30 μm and its width was about 0.5 cm.

2.2. CNT dispersion preparation and film deposition

In contrast to our previous spectroscopic study on CNT-based chemoresistors, where single-walled CNTs (purity $\geq$ 90%) with a mixture of chiralities (and thus both metallic and semiconducting characteristics) were employed [22],here we used chirality-sorted, highly enriched semiconducting single-walled CNTs (s-SWCNTs; chirality $\geq$ 95%, purity $\geq$ 95%, Merck, Darmstadt, Germany) for the fabrication of transistor-based gas sensors. This selection minimizes metallic percolation pathways and ensures improved device performance in CNT-TFT gas sensors, which depend on exponential current modulation and enhanced gate control. Following the protocol as in [14,28,29], a water-based dispersion of the SWCNTs was prepared using sodium carboxymethyl cellulose (CMC, Merck) as surfactant. Specifically, 0.05 wt% CNTs were dispersed in 0.5 wt% CMC aqueous solution. To promote dispersion, the mixture was sonicated (Fisherbrand FB-505, Fisher Scientific, Portsmouth, NH) using alternating cycles of 5 min at 50% and 30% power, for a total sonication time of 25 min. Subsequently, the solution was centrifuged (ThermoScientific SL 16, F15–6 rotor, Thermo Fisher Scientific, Waltham, MA) at 13000 rpm for 100 min, and the supernatant was diluted 1:30 in 1.3 mM CMC. Before CNT deposition, the fabricated devices were rinsed with isopropyl alcohol and deionized water, dried with compressed air, and treated with oxygen plasma to enhance surface wettability (1 min at 100 W). CNT films were deposited by spray-coating using an industrial air-atomizing spray valve (Nordson EFD, Westlake, OH) through a shadow mask, defining the active channel area. A total of 60 spray-coated CNT layers were deposited while maintaining the stage temperature at 70 °C throughout the deposition process. After deposition, the devices were immersed twice in deionized water (10 min each) at room temperature, followed by drying on a hot plate at 115 °C to remove the residual CMC surfactant. This milder aqueous post-treatment was adopted to preserve the integrity of the underlying Parylene-C dielectric, in contrast the harsher nitric acid processing used in previous CNT chemoresistor works.[13,14,22] The devices were stored under nitrogen in a glovebox until further use. Prior to SPEM/XPS measurements, the devices were introduced into a UHV chamber and annealed at 50 °C for 30 min to remove adsorbates and activate the surface. The morphology of chirality-sorted CNT films (95% purity) on unpatterned Si/SiO_2 substrates after CMC removal was examined by scanning electron microscopy (SEM) using a Thermo Scientific Helios 5 PFIB CXe (Fig. S1a, Supporting Information). Both chirality-sorted (95% purity) and chirality-mixed (90% purity) CNT films were deposited on unpatterned Si/SiO_2 substrates to compare their electronic properties by ultraviolet photoelectron spectroscopy (UPS), using a He-discharge lamp (He I, 21.22 eV; energy resolution 0.1 eV), a −7 V sample bias, and a VSW HA100 hemispherical analyzer (Fig. S1b and c, Supporting Information).

2.3. In-operando SPEM/XPS setup and ammonia dosing

In-operando SPEM and XPS measurements were carried out at the ESCA Microscopy beamline of the Elettra synchrotron, using a DHP system. This system enables the controlled delivery of short NH_3 pulses directly onto the device surface while maintaining UHV conditions in the analysis chamber. As demonstrated previously, this DHP

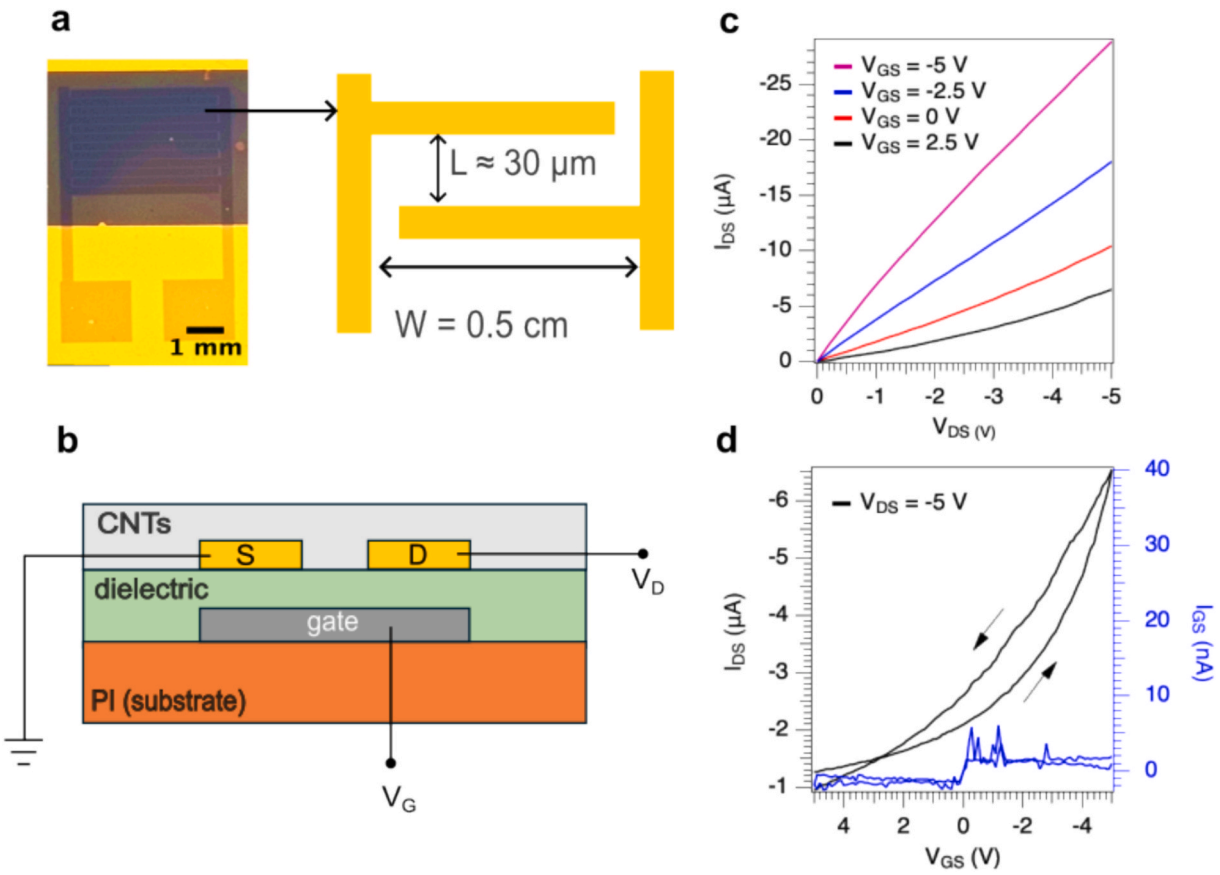

Fig. 1. A) optical micrograph of a flexible cnt-tft fabricated on apolyimide (PI) substrate and schematic illustration of the interdigitated source and drain electrodes, showing their geometry (channel length ≈ 30 µm, width ≈ 0.5 cm). b) Cross-sectional schematic of the device architecture, comprising a thick PI substrate, an aluminum gate electrode, a Parylene-C dielectric layer, and gold source and drain electrodes with a spray-coated CNT channel. c) CNT-TFT output characteristics (I_{DS} vs V_{DS}) for varying gate voltages (V_{GS}). d) Transfer characteristics (I_{DS} vs V_{GS}) at fixed drain bias (V_{DS}), confirming typical p-type transistor behavior.

configuration produces a locally high instantaneous NH_3 pressure at the sample surface (up to ~150 mbar) without compromising the overall chamber pressure (10^{-5}–10^{-6} mbar), thereby ensuring a sufficient electron mean free path for SPEM and XPS measurements [30,31]. NH_3 gas (≥ 99.5% purity) was delivered in pulses of ~3.4 ms duration at a repetition rate of 0.3 Hz, corresponding to a nominal NH_3 concentration of ~8 ppm at the sample surface. For SPEM mapping, the X-ray beam was focused to a spot size ~5 μm^2 to achieve spatially resolved contrast. For high-resolution XPS measurements, the beam was defocused to ~75 µm (beam spot diameter) to reduce the local photon density at the sample surface and ensure reliable spectral acquisition, with spectra collected while positioning the beam over the active CNT channel. The analyzer provided an energy resolution of 180 meV. Measurements were performed under two operating conditions: (i) the OFF state, with no biases applied, and (ii) the ON state, with a gate voltage of V_{GS} = -5 V and a drain voltage of V_{DS} = -5V, while the source was grounded.

3. Results and discussion

3.1. TFT characterization

The CNT-TFTs were characterized by measuring both output (Fig. 1**c**) and transfer curves (Fig. 1**d**). The device exhibited typical p-type CNT transistor behavior, with the drain-to-source current (I_{DS}) increasing under negative gate (V_{GS}) and drain-source (V_{DS}) bias. Notably, the device architecture enabled operation at voltage levels as low as 5 V, highlighting its potential for wearable gas-sensing applications. Nevertheless, some limitations were observed. In particular, the transistor did not fully reach the saturation regime (Fig. 1**c**), and current hysteresis appeared in the transfer characteristics (Fig. 1**d**). Further device optimization, particularly of the dielectric–active layer interface may reduce these effects in future work. Importantly, the linear-regime operation is consistent with the SPEM potential maps discussed below, which confirm a linear potential gradient and a steady-state current across the channel during NH_3 exposure. The SEM images of CNT films (see **Fig. S1a,b**, Supporting Information) reveal a more diluted network of CNTs compared to our previous work, [22] which can be attributed to the modified dispersion and deposition protocol adopted here to preserve the integrity of the pre-patterned device template. Despite this, the devices exhibit clear gate modulation of the drain current, confirming that the CNT network forms a functional percolating channel suitable for our *in-operando* investigation of gate-controlled gas-surface interactions while further device optimization falls beyond the scope of this surface science study.

3.2. SPEM surface potential mapping under source-drain bias

Scanning photoelectron microscopy (SPEM) experiments were first conducted without NH_3 dosing. A representative SPEM intensity map collected in the C 1s region while the device was in the OFF state is shown in Fig. 2**a**. Due to the geometrical configuration of the SPEM instrument, the recorded intensity maps capture both topographical and chemical information from the device surface [30,32]. Since the surface chemistry of the CNT film spray-coated across the entire device is expected to be uniform, the darker region observed in Fig. 2**a** is attributed primarily to topographical contrast and therefore corresponds to the CNT active channel, whereas the brighter regions correspond to the interdigitated source–drain electrodes. To disentangle topographical

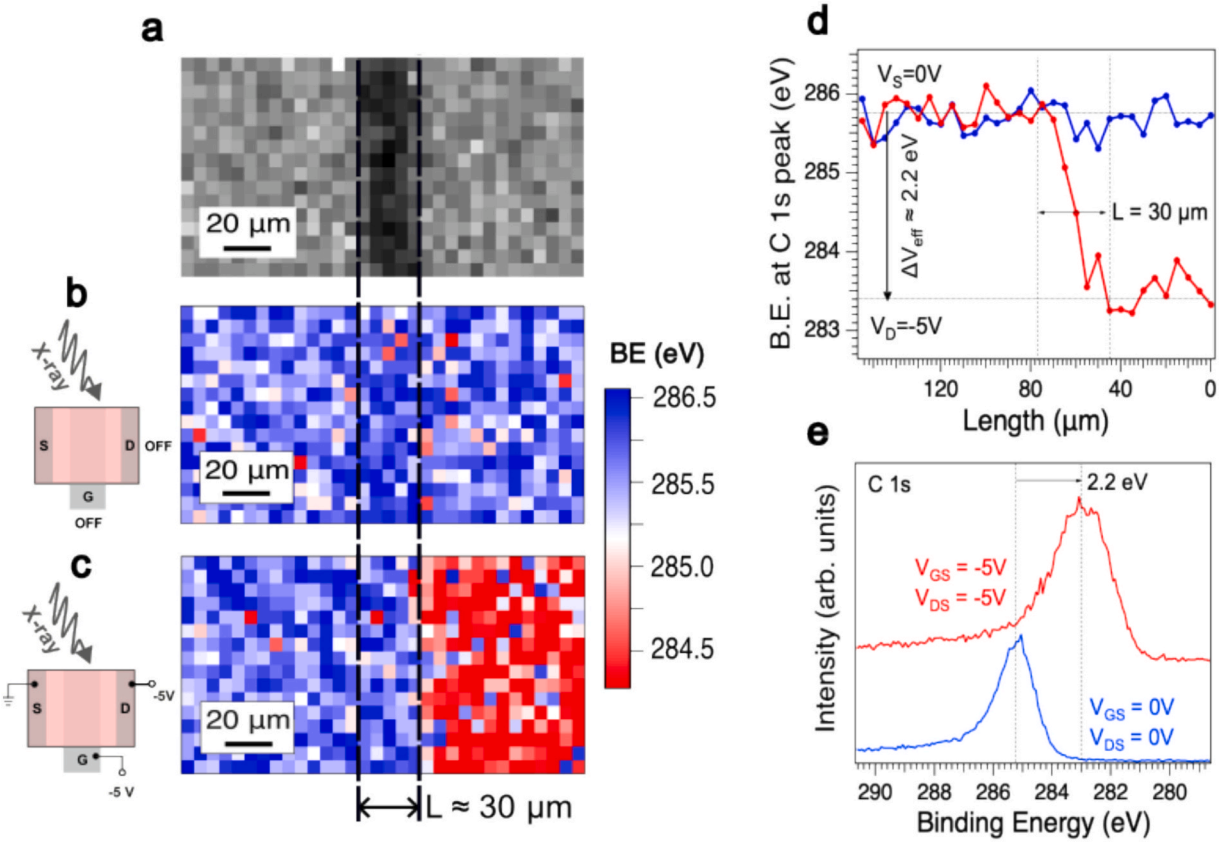

Fig. 2. A) spem image of the cnt-tft (off state) collected in the c 1s BE region, showing the spatial distribution of photoelectron intensity. The darker region corresponds to the CNT channel, while the brighter regions correspond to the interdigitated source and drain electrode regions. b) Corresponding OFF-state SPEM map of the surface electrostatic potential (pixel intensity converted to binding energy), showing an electronically homogeneous surface. c) Corresponding map of the device's ON state, revealing two distinct electrostatic regions due to the applied bias between source and drain. d) Averaged line profiles along the channel extracted from both OFF- and ON-state maps, showing for the ON state a linear potential gradient across the channel length (~30 µm). e) High-resolution C 1s spectra collected from the channel region in both OFF and ON states, showing a 2.2 eV shift toward lower BE under applied bias, consistent with the surface potential difference induced by the source–drain voltage.

from chemical contrast, the spatial intensity map in Fig. 2**a** was converted into a binding-energy-resolved map, where each pixel was reassigned to the BE corresponding to the maximum of the C 1s peak (see conversion procedure in **Fig. S2**, Supporting Information). The subsequent maps (Fig. 2**b, c**) display the spatial distribution of the C 1s BE across the device. Because shifts in the core-level BE are directly related to local variations in electrostatic potential, these maps qualitatively represent the surface electrostatic potential.

As expected, in the absence of applied voltages (OFF state), the electrostatic potential map of Fig. 2**b** displays a uniform electrostatic potential across the device, predominantly blue, corresponding to a BE of ~286 eV. In contrast, under applied bias (ON state), the corresponding map (Fig. 2**c**) reveals two distinct electrostatic regions, consistent with the potential difference between source (0 V) and drain (−5 V) contacts. An averaged line profile along the transistor channel (Fig. 2**d**) reveals a linear decrease in surface potential over approximately 30 µm, in excellent agreement with the device's channel length. This linear potential gradient qualitatively suggests a steady-state current flow characteristic of the linear regime of transistor operation [33], in agreement with the output and transfer characteristics shown in Fig. 1**c and 1d**.

Notably, the measured potential energy difference between source and drain was approximately 2.2 eV, which is about half of the expected 5 eV difference stemming from the applied bias. Since XPS is inherently surface-sensitive and the source–drain electrodes are buried beneath the CNT film, the measured binding-energy shifts could reflect changes in the electrostatic potential at the CNT surface rather than the potential of the underlying electrodes. Consequently, the observed surface potential difference may appear reduced relative to the applied bias, due to finite potential drops associated with contact resistances and the bulk resistance of the CNT channel.

High-resolution XPS spectra of the C 1s core level were acquired with the CNT-TFT in both OFF and ON states. As shown in Fig. 2**e**, the C 1s peak exhibits a pronounced shift of approximately 2.2 eV toward lower BEs when the CNT-TFT is in the ON state. This shift is consistent with the trend observed in the SPEM maps induced by the applied source–drain bias. In addition, comparison of the ON– and OFF-state spectra reveals a noticeable broadening of the C 1s peak in the ON state. This broadening can be attributed to the finite X-ray beam size (~75 µm spot diameter), which results in spatial averaging over regions of the channel experiencing slightly different electrostatic potentials.

3.3. *Gate-induced amplification of ammonia sensitivity*

As shown in Fig. 3, when the device is in the OFF state, the C 1s peak shifts by approximately 0.5 eV toward higher BEs upon NH_3 exposure. As reported in our previous work [22], this shift can be attributed to electron donation from NH_3 molecules to the CNTs, which depletes holes in the p-type CNT network and shifts the electronic states towards higher BE relative to the Fermi level.

Interestingly, in the CNT-TFT ON state, the C 1s peak exhibits a shift roughly twice as large, i.e., about 1.0 eV, toward higher BEs, which is consistent with the same electron-transfer mechanism as in the OFF state. However, the enhanced electron-transfer, and thus enhanced

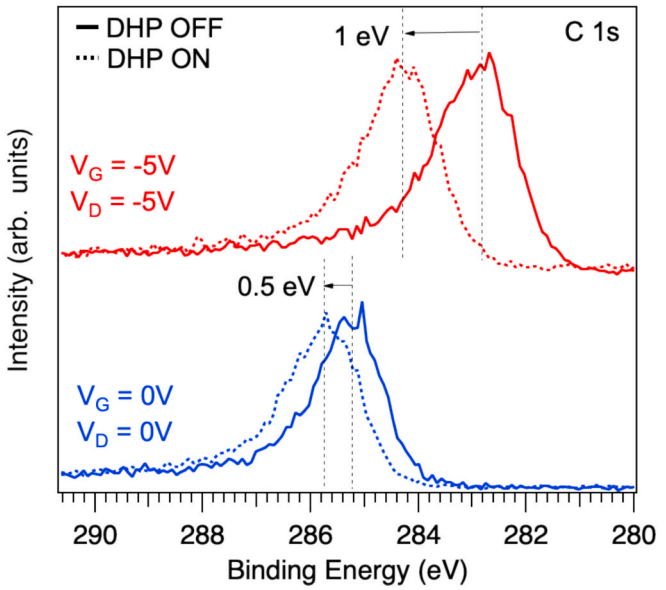

Fig. 3. High-resolution C 1s spectra of the CNT-TFT collected from the channel region in both OFF and ON states and w/o NH_3 dosing conditions. The lower spectra correspond to the OFF state without NH_3 dosing (solid blue line) and during NH_3 dosing (dashed blue line), whereas the upper spectra correspond to the ON state without NH_3 dosing (solid red line) and with NH_3 dosing (dashed red line). A clear shift of the C 1s peak toward higher binding energies is observed upon NH_3 exposure, with the magnitude of the shift approximately doubling under gate bias, indicating gate-modulated amplification of the CNT-TFT's chemical sensitivity.

response to NH_3, provides strong evidence of gate-modulated sensitivity in the ON state. Applying a negative gate voltage (−5 V) increases the hole concentration in the CNT channel, thereby enhancing the effect of electron donation from NH_3 as this leads to a larger observed BE shift in XPS.

This gate-modulated effect can be rationalized as follows: when an NH_3 molecule adsorbs on the CNT surface, it effectively acts as a transient dopant (electron donor). As discussed in previous theoretical studies, the formation energy of the dopant determines the efficiency of the charge-transfer event, and it depends directly on the position of the Fermi level relative to the band edges [34,35]. Applying a negative gate voltage shifts the Fermi level towards the valence band, increasing the hole concentration and thereby lowering the energetic barrier for electron transfer between NH_3 and CNTs. This enhances the overall efficiency of the charge-transfer process and, consequently, the overall chemical sensitivity of the CNT-TFT based sensor. Based on this Fermi-level-dependent mechanism, a systematic correlation between the magnitude of the gate bias and the C 1s BE shift is expected: increasingly negative gate voltages shift the Fermi level gradually closer to the valence band, further lowering the dopant formation energy and amplifying charge-transfer efficiency.

The electrical response of the CNT-TFT during NH_3 dosing in UHV shows a decrease in the source–drain current, consistent with the expected increase in resistance due to electron donation to the p-type CNT network. To contextualize these observations, it is worth discussing the nature of the NH_3–CNT interaction. Previous theoretical and experimental works have established that NH_3 interacts with pristine SWCNTs primarily through weak physisorption, governed by van-der-Waals forces and partial lone-pair donation from the nitrogen atom to the CNT π-system [36–38]. Supporting this picture, our previous *in-situ* XPS study on CNT-based chemoresistors [22], in which CNTs of ≥90% purity were used, demonstrated essentially fully reversible C 1s core-level shifts of approximately 1 eV upon NH_3 dosing, consistent with predominantly non-covalent, physisorptive interactions. The larger shift observed in that study compared to the ~0.5 eV shift measured here in the unbiased (OFF) state may, in part, reflect the higher defect density associated with the lower-purity CNTs used previously, suggesting that structural defects, including vacancies and residual oxygen containing functional groups (such as carboxylic and carbonyl species) introduced during CNT processing, can locally enhance NH_3 binding and shift the adsorption regime from physisorption toward weak or moderate chemisorption at specific sites [39]. However, despite the potentially stronger binding at such defect sites, the adsorption process in the previous work remained predominantly physisorptive, as evidenced by the essentially complete reversibility of the C 1s shifts upon gas removal. In the present work, where higher-purity SWCNTs (≥95%) are employed and therefore a smaller number of defect sites is expected, the recovery of the source–drain current after each NH_3 dosing cycle is nonetheless strongly suppressed, resulting in a dosimeter-like behavior (**Fig. S3**, Supporting Information). This is counterintuitive from a defect-density perspective as one would expect fewer defect-mediated binding sites and thus faster, more complete recovery. We therefore attribute the suppressed recovery to a combination of factors that are difficult to fully disentangle in the present study. The applied gate bias likely plays an important role, consistent with the enhanced charge-transfer efficiency discussed above, which may render NH_3 binding more favorable than desorption under negative gate bias. However, differences in device architecture, CNT processing protocol, and network morphology compared to our previous chemoresistor work [22] may also contribute, and the relative weight of each factor cannot be determined from the current data alone. A minor contribution from defect-mediated adsorption at residual sites within the spray-coated CNT network similarly cannot be excluded.

4. Conclusions

Overall, our results provide strong evidence for gate-modulated amplification of NH_3 sensitivity in CNT-based TFTs under NH_3 exposure. The fact that a negative gate voltage approximately doubles the BE shift (compared to the unbiased state) demonstrates that modulating the Fermi level can meaningfully lower the energetic barrier for charge transfer from adsorbed gas molecules to the semiconducting TFT channel. This observation bridges an important gap in the literature: whereas previous works have reported gate-dependent gas sensing via purely electrical readouts, they lacked insight into surface charge-transfer interactions. Systematic bias-dependent studies during gas exposure, extending beyond core-level shifts to valence band spectra and work function measurements, would be valuable future steps to explicitly map the relationship between gate voltage and BE shift, and to determine the thermodynamic limits of charge transfer as well as the adsorption and desorption kinetics governing sensor recovery. The present work establishes *in-operando* XPS/SPEM as a method capable of directly resolving the influence of gate voltage on surface charge-transfer interactions, an approach directly generalizable to various analyte gases and sensing materials.

From a broader perspective, our study underscores the advantage of combining surface-sensitive spectroscopy with electrostatic device gating under realistic operating conditions, providing a blueprint for the rational design of next-generation gated chemical sensors. While the present work demonstrates pronounced binding-energy shifts at ppm-level NH_3 concentrations, the same *in operando* SPEM/XPS approach can be extended to trace-level (sub-ppm or ppb) detection and to other gas analytes, such as NO_2 or volatile organic compounds, for which Fermi-level and gate modulation are expected to influence sensitivity. Moreover, investigations involving mixed analyte–oxygen environments may help clarify the role of adsorbed oxygen and competing surface processes under environmentally relevant conditions. In this context, the approach presented here offers a pathway to distinguish between weak physisorption, dynamic charge-transfer–induced surface charge accumulation, and stronger chemisorption processes in different sensing

materials. Finally, the demonstrated operation of flexible, polyimide-based CNT-TFTs at low gate voltages (± 5 V) highlights the potential for integrating such devices into wearable or portable sensing platforms. Overall, this work advances gas-sensing research by providing direct spectroscopic insight into gate-controlled sensing mechanisms, thereby extending the understanding beyond electrical characterization alone.

CRediT authorship contribution statement

Christos Gatsios: Writing – review & editing, Writing – original draft, Visualization, Methodology, Investigation, Formal analysis, Data curation. **Antonello Mascia:** Writing – review & editing, Methodology, Data curation. **Anna Goncharenko:** Writing – review & editing, Methodology, Data curation. **Cristian Tomasi Cebotari:** Writing – review & editing, Investigation. **Sahira Vasquez:** Writing – review & editing, Methodology, Data curation. **Niko Münzenrieder:** Writing – review & editing, Methodology. **Giulia Elli:** Writing – review & editing, Methodology. **Zygmunt Milosz:** Writing – review & editing, Methodology, Investigation, Data curation. **Matteo Amati:** Writing – review & editing, Methodology, Investigation, Data curation. **Luca Gregoratti:** Writing – review & editing, Methodology, Investigation, Data curation. **Luca Pasquali:** Writing – review & editing, Supervision, Funding acquisition. **Piero Cosseddu:** Writing – review & editing, Resources, Funding acquisition. **Luisa Petti:** Writing – review & editing, Resources, Funding acquisition. **Marco V. Nardi:** . **Melanie Timpel:** Writing – review & editing, Visualization, Supervision, Resources, Project administration, Methodology, Investigation, Funding acquisition, Conceptualization.

Declaration of competing interest

The authors declare that they have no known competing financial interests or personal relationships that could have appeared to influence the work reported in this paper.

Acknowledgments

The authors thank A. Pedrielli for his assistance in SEM imaging. This research was funded by the Italian Ministry of University and Research (MUR) through the PRIN 2022 Projects 2D-EMMA (Project n. 202289PMBP, CUP: B53D23004010006) and PETRA (Project n. 2022T7ZSEK, CUP: B53D23001860006). It also received funding from Next Generation EU through the PNRR 2023 Project NQSTI (Project n. PE0000023, CUP: B53C22004180005) and from the European Union Next-GenerationEU (PIANO NAZIONALE DI RIPRESA E RESILIENZA (PNRR)—MISSIONE 4 COMPONENTE 2, INVESTIMENTO 1.4—D.D. 1032 17/06/2022, CN00000022).

Appendix A. Supplementary data

Supplementary data to this article can be found online at https://doi.org/10.1016/j.apsusc.2026.167650.

Data availability

Data will be made available on request.

References

[1] Y. Luo, M.R. Abidian, J.-H. Ahn, D. Akinwande, A.M. Andrews, M. Antonietti, Z. Bao, M. Berggren, C.A. Berkey, C.J. Bettinger, J. Chen, P. Chen, W. Cheng, X. Cheng, S.-J. Choi, A. Chortos, C. Dagdeviren, R.H. Dauskardt, C. Di, M.D. Dickey, X. Duan, A. Facchetti, Z. Fan, Y. Fang, J. Feng, X. Feng, H. Gao, W. Gao, X. Gong, C. F. Guo, X. Guo, M.C. Hartel, Z. He, J.S. Ho, Y. Hu, Q. Huang, Y. Huang, F. Huo, M. M. Hussain, A. Javey, U. Jeong, C. Jiang, X. Jiang, J. Kang, D. Karnaushenko, A. Khademhosseini, D.-H. Kim, I.-D. Kim, D. Kireev, L. Kong, C. Lee, N.-E. Lee, P. S. Lee, T.-W. Lee, F. Li, J. Li, C. Liang, C.T. Lim, Y. Lin, D.J. Lipomi, J. Liu, K. Liu, N. Liu, R. Liu, Y. Liu, Y. Liu, Z. Liu, Z. Liu, X.J. Loh, N. Lu, Z. Lv, S. Magdassi, G. G. Malliaras, N. Matsuhisa, A. Nathan, S. Niu, J. Pan, C. Pang, Q. Pei, H. Peng, D. Qi, H. Ren, J.A. Rogers, A. Rowe, O.G. Schmidt, T. Sekitani, D.-G. Seo, G. Shen, X. Sheng, Q. Shi, T. Someya, Y. Song, E. Stavrinidou, M. Su, X. Sun, K. Takei, X.-M. Tao, B.C.K. Tee, A.-V.-Y. Thean, T.Q. Trung, C. Wan, H. Wang, J. Wang, M. Wang, S. Wang, T. Wang, Z.L. Wang, P.S. Weiss, H. Wen, S. Xu, T. Xu, H. Yan, X. Yan, H. Yang, L. Yang, S. Yang, L. Yin, C. Yu, G. Yu, J. Yu, S.-H. Yu, X. Yu, E. Zamburg, H. Zhang, X. Zhang, X. Zhang, X. Zhang, Y. Zhang, Y. Zhang, S. Zhao, X. Zhao, Y. Zheng, Y.-Q. Zheng, Z. Zheng, T. Zhou, B. Zhu, M. Zhu, R. Zhu, Y. Zhu, Y. Zhu, G. Zou, X. Chen, Technology roadmap for flexible sensors, ACS Nano 17 (2023) 5211–5295, https://doi.org/10.1021/acsnano.2c12606.

[2] R. Voggu, C.S. Rout, A.D. Franklin, T.S. Fisher, C.N.R. Rao, Extraordinary Sensitivity of the electronic structure and properties of single-walled carbon nanotubes to molecular charge-transfer, J. Phys. Chem. C 112 (2008) 13053–13056, https://doi.org/10.1021/jp805136e.

[3] R. Tang, Y. Shi, Z. Hou, L. Wei, Carbon nanotube-based chemiresistive sensors, Sensors 17 (2017) 882, https://doi.org/10.3390/s17040882.

[4] V. Schroeder, S. Savagatrup, M. He, S. Lin, T.M. Swager, Carbon nanotube chemical sensors, Chem. Rev. 119 (2019) 599–663, https://doi.org/10.1021/acs.chemrev.8b00340.

[5] N. Barsan, M. Schweizer-Berberich, W. Göpel, Fundamental and practical aspects in the design of nanoscaled SnO 2 gas sensors: a status report, Fresenius J. Anal. Chem. 365 (1999) 287–304, https://doi.org/10.1007/s002160051490.

[6] C. Wang, L. Yin, L. Zhang, D. Xiang, R. Gao, Metal oxide gas sensors: sensitivity and influencing factors, Sensors 10 (2010) 2088–2106, https://doi.org/10.3390/s100302088.

[7] Ammonia: International Chemical Safety Card (ICSC 0414), International Labour Organization (ILO) and World Health Organization (WHO), 2013. https://chemicalsafety.ilo.org/dyn/icsc/showcard.display?p_card_id=0414.

[8] M.-J. Chan, Y.-J. Li, C.-C. Wu, Y.-C. Lee, H.-W. Zan, H.-F. Meng, M.-H. Hsieh, C.-S. Lai, Y.-C. Tian, Breath ammonia is a useful biomarker predicting kidney function in chronic kidney disease patients, Biomedicines 8 (2020) 468, https://doi.org/10.3390/biomedicines8110468.

[9] A.C. Anand, S.K. Acharya, The Story of ammonia in liver disease: an unraveling continuum, J. Clin. Exp. Hepatol. 14 (2024) 101361, https://doi.org/10.1016/j.jceh.2024.101361.

[10] R. Upadhyay, T.P. Bleck, K.M. Busl, Hyperammonemia: what urea-lly need to know: case report of severe noncirrhotic hyperammonemic encephalopathy and review of the literature, Case Rep. Med. 2016 (2016) 1–10, https://doi.org/10.1155/2016/8512721.

[11] A. Nijkoops, M. Ciocca, M.A. Costa Angeli, S. Pogliaghi, S. Krik, E. Avancini, N. Münzenrieder, P. Lugli, L. Petti, Ammonia dynamics in the human body: insights in biomedical sensing technologies, Adv. Sens. Res. 4 (2025) 2400179, https://doi.org/10.1002/adsr.202400179.

[12] S. Vasquez, M.A.C. Angeli, A. Polo, A. Costantini, M. Petrelli, E. Avancini, R. Di Cagno, M. Gobbetti, A. Gaiardo, M. Valt, P. Lugli, L. Petti, In vitro gastrointestinal gas monitoring with carbon nanotube sensors, Sci. Rep. 14 (2024) 825, https://doi.org/10.1038/s41598-023-50134-z.

[13] S. Vasquez, M.A. Costa Angeli, M. Petrelli, M. Ahmad, B. Shkodra, B. Salonikidou, R.A. Sporea, A. Rivadeneyra, P. Lugli, L. Petti, Comparison of printing techniques for the fabrication of flexible carbon nanotube-based ammonia chemiresistive gas sensors, Flex. Print. Electron. 8 (2023) 035012, https://doi.org/10.1088/2058-8585/acef39.

[14] G. Elli, M. Ciocca, B. Shkodra, M. Petrelli, M.A. Costa Angeli, A. Altana, R. Carzino, D. Fragouli, L. Petti, P. Lugli, Electrolyte-gated carbon nanotube field-effect transistor-based sensors for nanoplastics detection in seawater: a study of the interaction between nanoplastics and carbon nanotubes, ACS Appl. Mater. Interfaces 16 (2024) 38768–38779, https://doi.org/10.1021/acsami.4c07692.

[15] J. Wang, H. Gong, F. Tian, Z. Li, J. Li, J. Jiang, Y. Li, X. Chen, Chemiresistive gas sensors: materials, mechanisms, and applications on the road to intelligence and multifunctionality, Small (2026) e12547, https://doi.org/10.1002/smll.202512547.

[16] K. Luo, H. Peng, B. Zhang, L. Chen, P. Zhang, Z. Peng, X. Fu, Advances in carbon nanotube-based gas sensors: Exploring the path to the future, Coord. Chem. Rev. 518 (2024) 216049, https://doi.org/10.1016/j.ccr.2024.216049.

[17] S.-X.-L. Luo, T.M. Swager, Chemiresistive sensing with functionalized carbon nanotubes, Nat. Rev. Methods Primer 3 (2023) 73, https://doi.org/10.1038/s43586-023-00255-6.

[18] A. Boyd, I. Dube, G. Fedorov, M. Paranjape, P. Barbara, Gas sensing mechanism of carbon nanotubes: from single tubes to high-density networks, Carbon 69 (2014) 417–423, https://doi.org/10.1016/j.carbon.2013.12.044.

[19] M. Salmeron, R. Schlogl, Ambient pressure photoelectron spectroscopy: a new tool for surface science and nanotechnology, Surf. Sci. Rep. 63 (2008) 169–199, https://doi.org/10.1016/j.surfrep.2008.01.001.

[20] A. Gurlo, R. Riedel, In situ and operando spectroscopy for assessing mechanisms of gas sensing, Angew. Chem. Int. Ed. 46 (2007) 3826–3848, https://doi.org/10.1002/anie.200602597.

[21] C. Baeumer, Operando characterization of interfacial charge transfer processes, J. Appl. Phys. 129 (2021) 170901, https://doi.org/10.1063/5.0046142.

[22] C. Gatsios, A. Mascia, C. Tomasi Cebotari, S. Vasquez, Z. Milosz, A. Pedrielli, M. Amati, L. Gregoratti, L. Petti, P. Cosseddu, L. Pasquali, M. Timpel, M.V. Nardi, Assessing the mechanism of NH_3 sensing in flexible carbon-nanotube-based chemoresistive sensors via in situ photoemission spectroscopy, Adv. Mater. Interfaces (2026) e00893, https://doi.org/10.1002/admi.202500893.

[23] H.-J. Shin, S.M. Kim, S.-M. Yoon, A. Benayad, K.K. Kim, S.J. Kim, H.K. Park, J.-Y. Choi, Y.H. Lee, Tailoring electronic structures of carbon nanotubes by solvent with electron-donating and -withdrawing groups, J. Am. Chem. Soc. 130 (2008) 2062–2066, https://doi.org/10.1021/ja710036e.

[24] A.M. Rao, P.C. Eklund, S. Bandow, A. Thess, R.E. Smalley, Evidence for charge transfer in doped carbon nanotube bundles from Raman scattering, Nature 388 (1997) 257–259, https://doi.org/10.1038/40827.
[25] J. Kong, N.R. Franklin, C. Zhou, M.G. Chapline, S. Peng, K. Cho, H. Dai, Nanotube molecular wires as chemical sensors, Science 287 (2000) 622–625, https://doi.org/10.1126/science.287.5453.622.
[26] S. Tripathy, A. Sett, S. Majumder, T.K. Bhattacharyya, Study of gate induced sensitivity amplification in carbon nanotube thin film transistor based ammonia sensor, Sens. Actuators B Chem. 382 (2023) 133511, https://doi.org/10.1016/j.snb.2023.133511.
[27] J. Song, D.-H. Kim, J. Tiepelt, Y.-M. Jo, G. McGrath, M. Song, T. Chen, J. Wang, A. Coto, S. Palani, D. Koh, S. Fuller, M. Shulaker, M. Dincă, M. Baldo, Tunable and highly sensitive functionalized carbon-nanotube-based integrated systems for chemical gas sensing, Nat. Sens. 1 (2026) 252–260, https://doi.org/10.1038/s44460-026-00037-z.
[28] G. Elli, S. Torkian, G. Ciccone, A. Rasheed, P. Lugli, L. Petti, P. Ibba, Flexible electrolyte-gated field-effect transistors for gallic acid detection, IEEE Sens. Lett. 9 (2025) 1–4, https://doi.org/10.1109/LSENS.2025.3572136.
[29] M. Petrelli, B. Shkodra, A. Falco, M.A. Costa Angeli, S. Vasquez, A. Scarton, S. Pogliaghi, R. Biasi, P. Lugli, L. Petti, Method for instability compensation and detection of ammonium in sweat via conformal electrolyte-gated field-effect transistors, Org. Electron. 122 (2023) 106889, https://doi.org/10.1016/j.orgel.2023.106889.
[30] M. Amati, M.K. Abyaneh, L. Gregoratti, Dynamic high pressure: a novel approach toward near ambient pressure photoemission spectroscopy and spectromicroscopy, J. Instrum. 8 (2013) T05001–T, https://doi.org/10.1088/1748-0221/8/05/T05001.
[31] M. Amati, L. Gregoratti, P. Zeller, M. Greiner, M. Scardamaglia, B. Junker, T. Ruß, U. Weimar, N. Barsan, M. Favaro, A. Alharbi, I.J.T. Jensen, A. Ali, B.D. Belle, Near ambient pressure photoelectron spectro-microscopy: from gas–solid interface to operando devices, J. Phys. Appl. Phys. 54 (2021) 204004, https://doi.org/10.1088/1361-6463/abe5e2.
[32] L. Gregoratti, A. Barinov, E. Benfatto, G. Cautero, C. Fava, P. Lacovig, D. Lonza, M. Kiskinova, R. Tommasini, S. Mähl, W. Heichler, 48-Channel electron detector for photoemission spectroscopy and microscopy, Rev. Sci. Instrum. 75 (2004) 64–68, https://doi.org/10.1063/1.1630837.
[33] S. Kasap, Principles of Electronic Materials and Devices, McGraw-Hill Inc, USA, 2006.
[34] A. Zunger, O.I. Malyi, Understanding doping of quantum materials, Chem. Rev. 121 (2021) 3031–3060, https://doi.org/10.1021/acs.chemrev.0c00608.
[35] C. Freysoldt, B. Grabowski, T. Hickel, J. Neugebauer, G. Kresse, A. Janotti, C. G. Van De Walle, First-principles calculations for point defects in solids, Rev. Mod. Phys. 86 (2014) 253–305, https://doi.org/10.1103/RevModPhys.86.253.
[36] J. Zhao, A. Buldum, J. Han, J.P. Lu, Gas molecule adsorption in carbon nanotubes and nanotube bundles, Nanotechnology 13 (2002) 195–200, https://doi.org/10.1088/0957-4484/13/2/312.
[37] S. Peng, K. Cho, Ab initio study of doped carbon nanotube sensors, Nano Lett. 3 (2003) 513–517, https://doi.org/10.1021/nl034064u.
[38] C.W. Bauschlicher, A. Ricca, Binding of N H 3 to graphite and to a (9,0) carbon nanotube, Phys. Rev. B 70 (2004) 115409, https://doi.org/10.1103/PhysRevB.70.115409.
[39] J. Andzelm, N. Govind, A. Maiti, Nanotube-based gas sensors – role of structural defects, Chem. Phys. Lett. 421 (2006) 58–62, https://doi.org/10.1016/j.cplett.2005.12.099.